Advanced Course and Workshop on Blood Flow
BF 2005 – (pp.243–271) – Warsaw, 2005.

# Do Doppler Systems Color Arteries Red?

Arnold P.G. Hoeks[1] and Robert S. Reneman[2]

*Cardiovascular Research Institute Maastricht (CARIM)*
[1]*Dept. Biophysics, CARIM*
[2]*Dept. Physiology, CARIM*
*University Maastricht*
*PO BOX 616, 6200 MD Maastricht, the Netherlands*
[1]*A.Hoeks@bf.unimaas.nl*
[2]*R.Reneman@fys.unimaas.nl*

Ultrasound techniques provide in real-time detailed information about the structure and hemodynamic functioning of the cardiovascular system. The Doppler technique, either continuous wave (CW) or pulsed, facilitates direct measurement of the time-dependent blood velocity at a specific site. The gradual development of Doppler techniques from the "simple" CW systems to advanced color Doppler systems has expanded the possibilities to relate deviant blood flow velocity behaviour to changes in structure and functioning of the vessel wall. This chapter will discuss in detail the signal analytic aspects of Doppler instrumentation, and address the trade-offs and the interrelationships between resolution in the time, spatial and frequency domain.

Key words: *Doppler systems, instrumentation, velocity estimation, signal processing*

## 1. Introduction

Since the introduction of ultrasound Doppler systems for human applications in 1960 by Satomura [1] and coincidentally by Franklin [2], the Doppler technique to estimate the blood velocity pattern gradually gained an established place in the assessment and evaluation of the dynamic characteristics of the arterial and venous circulation and in the diagnosis of vascular disorders. To appreciate its value in clinical practice, as will be demonstrated in the accompanying chapters, we will first address the concept and evolution of Doppler systems and demonstrate their applicability by providing a few examples.

If sound waves with a frequency $f_e$ are reflected by a moving acoustical interface, then the interface will induce a shift $f_d$ in the sound frequency proportional to the velocity $v$ of the interface. This is known as the Doppler principle [3], originally described for light. It was the Dutchman Buys Ballot who described the phenomenon for sound waves, [4] after an attempt to falsify the concept for sound using musicians with absolute hearing and a moving train. To demonstrate the principle, consider a single wave impinging perpendicularly on an interface with velocity $v$ in the same direction as the incident sound. The wave will have a velocity relative to the interface of $c+v$, while after reflection the relative velocity is changed to $c-v$ with $c$ being the speed of sound in the medium. The time required for total reflection of one wavelength $\lambda$ equals $\lambda/(c+v)$. In the meantime the front of the wave has covered a distance $\lambda'$ with $\lambda'(f_e+f_d)=c$ and $\lambda f_e = c$. Solving the above relations for $f_d$ results in $f_d = 2f_e v/(c-v)$. Since $c$ in tissue is far much greater (about 1500 m/s) than blood velocities ($v$ will generally not exceed 1 m/s) the expression may be simplified to $f_d = 2f_e v/c$ for applications in flowing blood. If the paths of the interface (Fig. 1) and of the sound waves are inclined with respect to each other, with an enclosed angle $\alpha$, the interface velocity with respect to the sound waves will be reduced to $v\cos\alpha$ and the expression becomes

$$f_d = \frac{2f_e v\cos\alpha}{c}\,. \tag{1.1}$$

For blood flow examinations transducers are employed to convert electric signals to sound and the reflected and backscattered signal to electric signals. Only the velocity component relative to the sound transducer (emitter and receiver) contributes to the Doppler effect (Fig. 1). If the enclosed angle is 90° (perpendicular observation), the Doppler shift frequency will be zero, while for angles between 90° and 270° the shift frequency will be negative.

Assuming a relative velocity of blood of $v = 1$ m/s and an emission frequency of 5 MHz the Doppler shift frequency will be $f_d = 6.1$ kHz ($c = 1500$ m/s). Generally, blood flow velocities are below 1 m/s, only in and im-

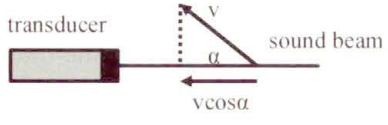


FIGURE 1. Only the velocity component relative to the transducer contributes to the Doppler effect.

mediately distal to a stenosis velocities up to 5 m/s may be reached. Hence, the Doppler shift frequencies are in the audio range and can be evaluated aurally.

Angles unequal to zero will only lead to a received signal, if the dimension of the reflector is small with respect to the wavelength of the ultrasound used, causing scattering of the sound in all directions. This requirement is met by the red blood cells with an ellipsoid dimension of 5–8 $\mu$m. If they travel with different velocities, then also a spectrum of Doppler frequencies rather than a single frequency component will be received [5]. From a physical and statistical point of view this is too simplistic because, due to the tight packing (6 million cells per mm$^3$), for any blood cell another can be found in the direct neighborhood that will cancel the backscattered wave. However, for blood flows the Doppler effect originates from variations in packaging density rather than from individual cells.

Although the concept of Doppler systems seems to be rather simple, they heavily rely on basic signal analysis concepts. The most fundamental one is the relation between the effective signal bandwidth $B$ and the effective duration $T$ of the corresponding impulse response [6]: BT$\geq$ 0.5. The effective bandwidth is defined as the square root of the mean squared deviation of the central frequency; the same definition applies to the effective duration of the impulse response. The minimum value of 0.5 for the time-bandwidth product is attained for a Gaussian shaped spectral distribution (the corresponding impulse response is then also Gaussian shaped). In daily practice the above rule is simplified to BT= 1 with $B$ and $T$ the width of the spectral distribution and the impulse response at half the maximum value, respectively (Fig. 2). For a bandpass filter with a width of 2 MHz the duration will be 0.5 $\mu$s and increasing the bandwidth will reduce the duration. For a low-

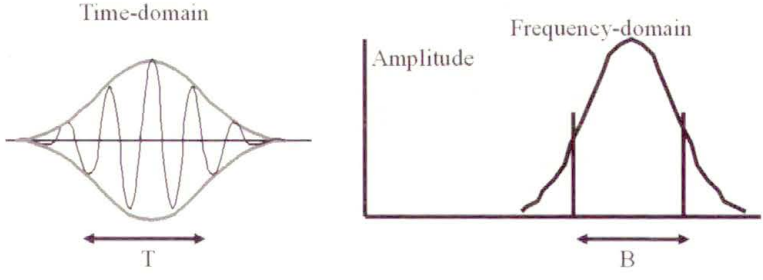


FIGURE 2. The product of the duration T and bandwidth B is approximately 1.

pass filter both positive and negative frequencies should be considered, which results in a bandwidth of twice the cut-off frequency.

As indicated above, an observation interval $T$ allows a frequency resolution of $\Delta f$ Hz. Recalling the Doppler equation (Eq. (1.1)), a spectral resolution of $\Delta f_d$ relates to a velocity resolution $\Delta v$ as:

$$\Delta f_d = \frac{2 f_e \Delta v \cos\alpha}{c} \quad \text{or} \quad \Delta v = \frac{c}{2 T f_e \cos\alpha} \,. \tag{1.2}$$

Hence, for the same observation interval $T$ the velocity resolution will improve with a higher emission frequency (or an observation angle close to zero). On the other hand, in tissue the sound energy relative to emitted energy decreases proportional with the sound frequency and the path, setting an upper bound on the incident frequency.

In vascular studies and in vascular medicine the blood velocity is measured by placing a probe, containing the transducers for emission and reception of ultrasound, on the skin. The direction of the probe is interactively varied to locate an artery until a balance is found between the amplitude and the pitch of the Doppler ultrasound. As we will show, an important class of Doppler systems needs only one transducer, acting alternatively as emitter and receiver.

## 2. Continuous Wave (CW) Systems

### 2.1. Hardware Configuration

The simplest configuration to extract the Doppler shift information from the blood velocity distribution is a Continuous Wave (CW) system. It employs separate transducers (Fig. 3) for emission and reception of ultrasound (although theoretically also a single transducer would suffice). The sensitivity range of the probe is confined within the intersection of the emitted beam

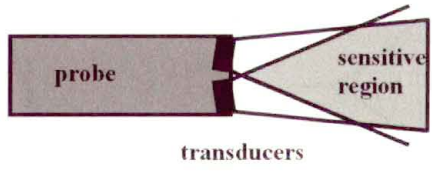


FIGURE 3. A CW probe has separate transducers for continuous emission and reception of ultrasound waves. The sensitive region of the probe is where both beams overlap.

and the sensitivity range of the receiver crystal (Fig. 3). Hence, the sample volume of a CW Doppler system is quite large and does not convey information about the depth the Doppler signals are originating from. On the other hand the system exhibits a high sensitivity, making it easy to locate a vessel of interest by listening to the Doppler sound. Nowadays the Doppler unit to emit and process the received signal is the size of an average sized calculator and is therefore popular by medical doctors to check rapidly whether an artery is still patent.

Before we go into the details of signal processing in Doppler systems, we will first discuss the concept of complex signals, which can be considered as an extension of real signals as we observe in common life. Any cosine (or sine) wave is described by its amplitude $A$ and frequency $\omega$, e.g. the signal $s(t) = A\cos(\omega t)$, where $t$ denotes time. The argument of the cosine is also called the (instantaneous) phase of the signal. Since $s(t)$ has 2 degrees of freedom it is impossible to extract unambiguously the current phase or amplitude from a sample (or a few samples) of an unknown signal. This problem is solved by considering the sample as a projection of a complex signal on the (real) x-axis (Fig. 4). The sequence of x-axis samples is called the in-phase signal as opposed to the sequence of the corresponding projections on the y-axis (imaginary axis) denoted as in-quadrature signal. The amplitude of the signal is the radius (the square root of the sum of squares of the real and imaginary signals), while the instantaneous phase follows from the arctangent of the imaginary and real component. The combination of a real and imaginary signal is called a complex signal. The in-quadrature signal is derived from

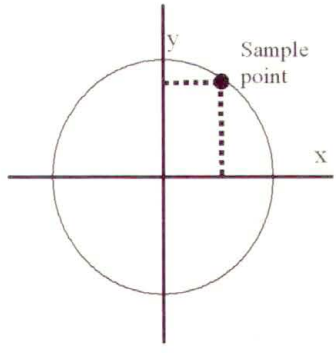


FIGURE 4. A complex signal is composed of a real (in-phase) and an imaginary (in-quadrature) component.

the in-phase signal by shifting the phase over 90 degrees independent of the frequency, i.e. the cosine-component is converted into a sine-component. This can be accomplished in the time-domain as well as in the frequency domain. A complex signal is commonly denoted as $s(t) = A(t)\exp(j\omega t) = A(t)(\cos(\omega t) + j\sin(\omega t))$, with $A(t)$ the amplitude of the envelope of the signal, $\omega = 2\pi f$ the angular frequency and $j$ the symbol for the complex component.

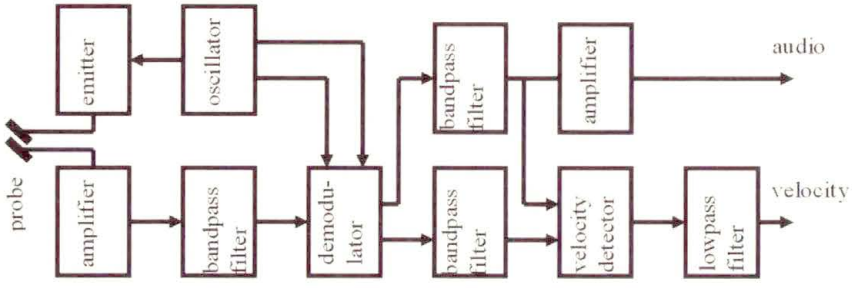


FIGURE 5. Block diagram of CW Doppler system

The basic configuration of a CW Doppler system is depicted in Fig. 5. An internal oscillator provides the emitter amplifier with a sine wave with a constant amplitude and frequency, the emission frequency. The receiver amplifier has a large dynamic range to accommodate the large echoes from structures, e.g. vessel walls, as well as the low amplitude signals backscattered by the red blood cells. The bandpass filter suppresses all noise in the received signal outside the bandwidth of interest (30 kHz) to improve the signal to noise ratio (SNR). The demodulator is a crucial element in Doppler systems, because it shifts the frequency spectrum centered at the emission frequency to zero frequency by multiplying its input signal $r(t) = A(t)\cos((\omega_e + \omega_d)t)$ by the quadrature oscillator signal:

$$\begin{aligned} d(t) &= r(t)\{\cos(\omega_e t) + j\sin(\omega_e t)\} = A(t)\cos((\omega_e + \omega_d)t)\{\cos(\omega_e t) + j\sin(\omega_e t)\} \\ &= 0.5A(t)[\cos(\omega_d t) + \cos((2\omega_e + \omega_d)t) + j\{\sin(\omega_d t) + \sin((2\omega_e + \omega_d)t)\}]. \end{aligned} \tag{2.1}$$

The imaginary (labeled with $j$) and real components are processed by separate channels. The signal components at a double emission frequency are effectively suppressed by a lowpass audio filter with a cut-off frequency of about 15 kHz, depending on the emission frequency employed and the

anticipated maximum velocity. The demodulation process as indicated in Eq. (2.1) applies for all frequency components the received signal is composed of, so also for a signal with zero or a very low Doppler frequency, presumably originating from stationary or slowly moving structures, e.g. vessel walls. Reflections of the latter may have amplitudes exceeding the amplitude of blood induced signals by at least a factor of 100 (40–60 dB). To suppress these low frequencies the audio filter is converted to a bandpass filter, where the lower cut-off frequency (in the range of 300 to 600 Hz) sets also a lower bound for the (blood) velocities that can be detected. If this cut-off frequency is set too low the echoes from strongly reflecting structures will interfere with and may even temporarily dominate the audio signal to determine [7]. Generally the wall filter can be set at a lower value for the same emission frequency, if venous flows are investigated.

## 2.2. Audio Evaluation

The demodulated bandpass filtered quadrature signals contain Doppler shift frequencies in the audio range. Both quadrature channels sound exactly the same. Aural evaluation may be impaired if the Doppler information of both a vein and an artery is conveyed. However, generally the vein and artery will have an opposite flow direction with respect to the probe. Under this condition the arterial and venous signals can be separated by a proper combination of the quadrature signals (Fig. 6). The cosine function is even, i.e. $\cos(-\omega_d) = \cos(\omega_d)$, while the sine function is odd, i.e. $\sin(-\omega_d) = -\sin(\omega_d)$. Phase shifting the cosine over 90 degrees independent of frequency (Hilbert filter) yields a sine component with the same sign as the quadrature compo-

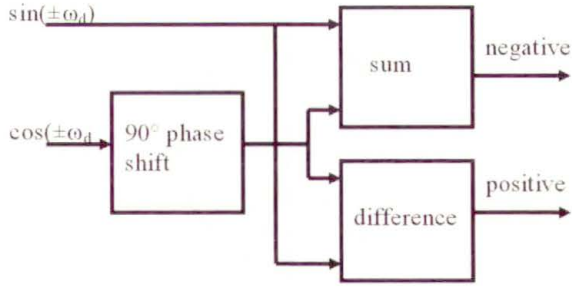


Figure 6. With a 90° phase shifter separate audio-outputs for positive and negative Doppler frequencies can be derived from the quadrature Doppler signal.

nent for positive frequencies, but an opposite sign for negative frequencies. Hence, the sum will give only an output for positive frequencies, while the difference becomes non-zero for negative frequencies. In this way velocity direction information is recovered.

### 2.3. Velocity Estimation

An important characteristic of a Doppler system is its capability to estimate the instantaneous frequency averaged over a short interval (e.g. 20 ms) within the observed region [8]. The Doppler equation relates the average frequency to an average (blood) velocity. Usually in CW Doppler systems the principle of a zero crossing counter is used to estimate the average frequency. For this purpose only the sign of the quadrature signals is retained, so at any instant it is only known in which quadrant the phase vector is located, but its precise direction (phase) remains unknown (Fig. 7). If the phase vector changes from the third to the fourth quadrant only the in-phase component will change sign from negative to positive. Under that condition a short (0.1 ms) positive pulse is generated. Alternatively, if the in-phase component changes sign in the reverse direction, while the in-quadrature component remains negative, i.e. the phase vector moves from the fourth to the third quadrant, a negative pulse is generated. Subsequently the positive and negative pulses are low pass filtered with a cut-off frequency of about 20 to 30 Hz (response time 50 to 30 ms), yielding a velocity output (after proper calibration) as a continuous function of time. The filter process may be applied to the sum of positive and negative pulses or for both outputs separately. One should realize that the sum of the velocity outputs is not equal to the velocity of the summed outputs, because in the first case the amplitude information

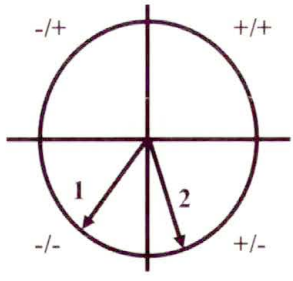


FIGURE 7. A quadrature sign processor (zero crossing detector) allows detection of velocity direction.

is not properly taken into account. The output of a zero crossing detector is only accurate for signals wit a narrow bandwidth with respect to the center frequency, but the error will be substantial (10%) for wide band signals [9, 10]. Moreover, under poor signal-to-noise conditions large errors may occur, especially for zero crossings detectors acting on only a one-way phase shift direction. We will later discuss a more advanced option to estimate the average velocity.

### 2.4. Spectral Analysis

Any signal in the time domain can be decomposed into its constituent components in the frequency domain (Fourier analysis). To allow proper interpretation the signal should be stationary within a given time window, i.e. its statistical characteristics should be constant. Due to the pulsatile nature of blood flow, Doppler signals only comply with this requirement for a short period of time. Therefore the quadrature Doppler signal is broken down into short segments of 10 ms that are subjected to Fourier analysis. For that purpose the quadrature signals are sampled and converted to digital numbers at a sample frequency, which should be at least twice the maximally anticipated frequency to avoid aliasing. In the latter case the phase vector would rotate over more than 180° (Fig. 7), which would be interpreted as a phase shift of less than 180° in the opposite direction. The observed Doppler frequency then deviates in magnitude and in sign from the original one. The spectral amplitude distribution of the subsequent time segments constitutes the spectrogram with on the horizontal axis time and on the vertical axis the (Doppler) frequency. The amplitude of each spectral component is displayed as shades of grey [5, 11]. The selected length of the time window dictates the width of each spectral bin (spectral resolution); for 10 ms segments this will be 100 Hz. Increasing the length of the time segments will improve resolution at the expense of blurring the time-dependent features of the signal, e.g. acceleration time. To avoid this problem the time segments are normally half-overlapping, resulting in twice as many spectra for the same total length of the signal. Spectral analysis is rather insensitive to the signal-to-noise ratio. Even if the SNR= 1, the spectral distribution of the Doppler signal will remain clearly visible in the spectrogram. This is due to the fact that the noise will evenly be distributed over the entire spectral range, while the Doppler signal will be concentrated within a relatively small frequency band.

As blood flow accelerates from end-diastole to peak-systole the number of observed blood cells will remain more or less the same and one would expect that the Doppler signal amplitude will hardly change. However, the increased friction on blood cells due to shear stresses causes spatially a more inhomogeneous density distribution and a concomitant increase in amplitude [12–14]. On the other hand, in the frequency domain in peak-systole the signal power is distributed over a larger range, causing a substantial modulation of the spectral amplitude over the cardiac cycle. This modulation is attenuated by displaying the logarithm of the spectral amplitude with the additional advantage that the appearance of the spectrogram is rather insensitive for the gain settings.

A common parameter to extract from the spectrogram is the frequency envelope because it is rather insensitive to the observed velocity distribution and noise [15, 16]. However, there never is a sharp cut-off for the maximum frequency. The sensitive region of a Doppler system depends on the local shape of the ultrasound beam and, for pulsed Doppler systems, the axial length of the sample volume (see next section). The transit time depends on the path of the scatterers through the sensitive region and the velocity. Because of the time bandwidth product the transit time will cause blurring of the frequency spectrum (geometric broadening) which will vary throughout the cardiac cycle. For pulsed Doppler systems operating with an emission burst of 6 periods the blurring may amount to 16% of the peak frequency corresponding to the maximum velocity. In the past, several maximum frequency estimators have been proposed [17–21] and each of them use some arbitrary criterion for the maximum frequency with respect to the spectral Doppler amplitude and the noise background.

## 3. Pulsed Doppler Systems

CW Doppler systems have the advantage that they have an unlimited velocity range and that they are easy to use. On the other hand they have a poor range selectivity which makes them less suited for regions with different flow patterns, e.g. cardiac cavities or extremities where the arterial blood flow may reverse in end-diastole. Pulsed Doppler systems, like echo systems, allow the interrogation of the blood flow at a selected depth. Moreover, they can easily be combined with echo systems to provide visual feedback about the site of measurement.

The concept of pulsed Doppler systems is based on the notion that signals are fully determined by samples provided that, according to the Nyquist theorem, the sample frequency exceeds twice the maximally anticipated signal frequency (see previous section). This observation implies that the received signal intermittently rather than continuously can be applied to the input of the demodulator (Fig. 8), or that the ultrasound can be emitted in bursts, with a corresponding increase in bandwidth of the receiver filter. Because the signal from the selected depth range is only intermittently present at the output of the demodulator, it has to be captured with a sample-and-hold to retain the value until it is updated in the next reception cycle (Fig. 8).

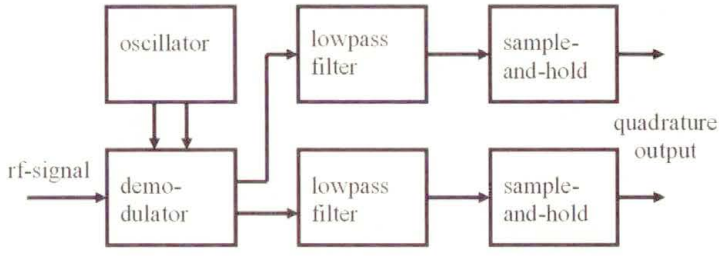


FIGURE 8. Demodulator of a pulsed Doppler system

The function of the lowpass filters following the demodulator is the same as those for a CW system (to remove the double emission frequency), but the design is completely different. Because it has to accommodate short bursts, the bandwidth should be enlarged considerably. Let us assume a burst of 6 periods, then the fractional bandwidth (bandwidth divided by center frequency) of the received radio-frequency (rf) signal equals 1/6. A fourth order characteristic provides a roll-off of 24 dB/octave, so the filter will reach an attenuation of about 70 dB at the center frequency. This is sufficient regarding the dynamic range of the received signal, which will be of the same order. Shorter bursts would even require a sharper roll-off. However, in practice longer bursts up to 10 periods will be used in pulsed Doppler mode to avoid the effect of depth-and-frequency depending attenuation on the center frequency. The sample-and-hold is activated at a preset delay with respect to the time of emission, corresponding to the desired depth of interest, and acts as a gate for the demodulated and filtered signal. As stated, the active length of the gate is given by the bandwidth of the lowpass filter, which was set according to the burst length used. This also sets the axial length of the sample

volume while its lateral dimensions are determined by the local shape of the ultrasound beam [22]. It should be stressed that the demodulator of a pulsed Doppler system cannot detect the Doppler shift, because of the short observation time. Instead it provides the phase of the rf-signal with respect to the oscillator reference signals. The phase gradually changes with depth rather than due to motion. Only the output of the sample-hold reveals the Doppler signal. It has a staircase appearance and is directly suited for conversion to digital format to perform wall filtering. In a digital filter the cut-off frequency is directly related to its update frequency, i.e. the pulse repetition frequency (PRF) of the pulsed Doppler system.

A pulsed Doppler system samples the Doppler signal from a specific depth at a rate equal to the PRF of the system. This is sufficient to accommodate without aliasing Doppler signals from physiological flows (peak velocities up to 1.5 m/s) but inappropriate for pathophysiological velocities as in arterial stenoses or stenosed cardiac valves. Aliasing will show up on the spectrogram as a roll-over: frequencies exceeding the upper limit of PRF/2 will appear at the bottom near −PRF/2 and vice versa. This can easily be solved by shifting the baseline upward or downward, depending on the direction requiring the largest range. Baseline shifting will extend the frequency range to maximally PRF, but then the flow should remain unidirectional. Some systems provide a further extension by the high PRF (Hi-PRF) option. Let us assume that the system is suited (depth attenuation) and set for flow velocity assessment at a depth of 10 cm. Doubling the PRF and halving the depth delay to 5 cm will force the system to sample the signals from a depth of 5 cm with respect to the current emission and from a depth of 10 cm with respect to the previous emission. If the region at 5 cm does not contain flow, then the Doppler signal is appropriately obtained from a depth of 10 cm at a double rate, thereby extending the velocity range. The drawback is that the depth-depending gain only operates over a short range, putting a high demand on the dynamic range of the system, especially if the PRF is tripled or quadrupled.

If the Doppler signals are retained in their sampled (digital) form, then a zero crossing counter is unsuited to estimate the average Doppler frequency, because transitions over 2 quadrants may occur. In 1985 Kasai proposed an alternative based on the argument of the autocorrelation $C(1)$ at lag 1 of the

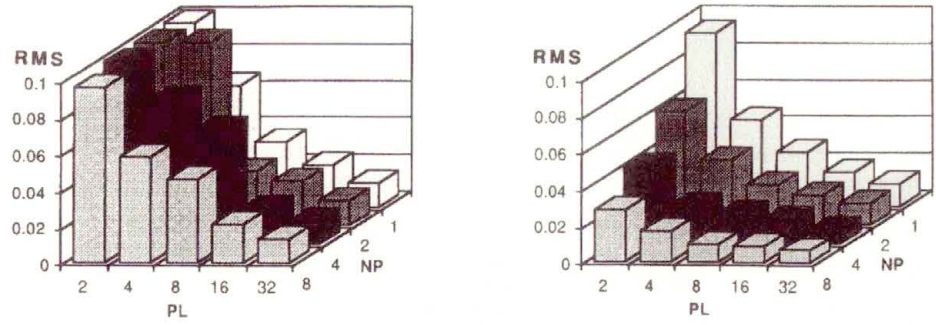


FIGURE 9. The RMS error (λPRF) of the standard pulsed Doppler velocity estimate (left picture) does not vary with the number of periods (NP) but improves with increasing package length (PL) while the velocity estimate based on cross-correlation (Sec. 5) of the radio-frequent (rf) signal improves with both PL and NP for a signal with a fractional bandwidth of 0.25, SNR= 10 dB, mean velocity is 0, and width velocity distribution 0.1 λPRF.

sampled quadrature Doppler signals $d(t)$, [23]:

$$C(1) = \frac{1}{\mathrm{PL}-1} \sum_{j=1}^{\mathrm{PL}-1} d^*(j)d(j+1). \tag{3.1}$$

In Eq. (3.1) PL is the package length (the number of Doppler signals considered) and $d^*(j)$ is the conjugate of $d(j)$, i.e. the sign of the imaginary part is reversed. As expected the precision of the velocity estimate decreases with the square root of the package length (Fig. 9). Only for a SNR$<$ 10 dB, a short package length (PL$\leq$10), a mean velocity close to PRF/2 and a moderate width of the velocity distribution (0.2PRF) the precision may be poorer than 10% of the PRF, but for most conditions the precision will be better than 5% of the PRF [24–26]. Unlike the zero-crossing meter, the approach of the complex autocorrelator still functions properly if the instantaneous frequency exceeds PRF/2, provided that the velocity averaged over the time window is not subject to aliasing. To maintain the dynamic characteristics of the velocity waveform, the observation window should be about 10 ms, which converts to a package length of 100 for a PRF of 10 kHz (maximum depth 7.5 cm). This quite large number ensures precise detection of the average velocity, even if sophisticated wall suppression filters, like singular value decomposition, are applied [27, 28].

## 4. Multigate Pulsed Doppler Systems

The digital and computer techniques, emerging in the 1980's, facilitated reliable data processing of the sampled Doppler signals, e.g. vessel wall suppression, mean velocity detection and spectral analysis. The associated high processing power allowed to integrate parallel processing channels for each sample volume into single circuitry with serial processing, accommodating many sample volumes. Given this technology it was a small step to extend the number of consecutive sample volumes drastically to 64 and even 128 samples along a line of insonation [29–31]. A prerequisite is a large dynamic range for the analog-to-digital conversion of the outputs of the demodulator (Fig. 8) because at that stage the weak Doppler signals from blood particles are still mixed with the large amplitude echo signals from stationary and slowly moving structures like vessel walls. A total dynamic range of 72 dB (12 bits) allows for echo signals that are a factor 100 (40 dB) to 1000 (60 dB) stronger than blood Doppler signals without saturating the analog-to-digital converter. With multigate Doppler systems one can measure the time-dependent velocity distribution over the cross-section of an artery lumen as a function of time [32, 33].

The detail of the eventually obtained instantaneous velocity distribution largely depends on the spatial resolution that can be attained. As stated before a short duration of the emitted acoustic pulse requires a large bandwidth, which enlarges the effects of depth- and frequency dependent attenuation. Hence, the central frequency of the received signals will be shifted down; consequently the velocity will be overestimated (Eq. (1.1)). To solve this problem, the local central frequency of received radio frequent (rf) signals is estimated simultaneously [25, 34], using autocorrelation of the demodulated rf signals with depth lag 1 (Eq. (3.1)) over short depth segments. However, the required roll-off of the phase detection filters following the demodulators sets a lower bound for the pulse duration. This is why preference is given to direct processing of the rf signals. One should realize that not only the pulse duration but also the local beamwidth in combination with the angle of observation affect the radial resolution of the velocity estimate. For an angle of 60°–70° between flow direction and the incident beam it does not have sense to make the pulse much smaller than 1/4 of the local beamwidth (Fig. 10); further shortening will hardly affect the observed range in the radial direction of the blood vessel.

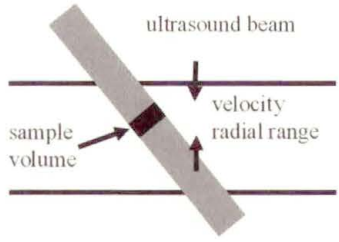


FIGURE 10. The spatial resolution in the radial range is affected by both the axial (length sample volume) and lateral (local beamwidth) resolution of the ultrasound system.

## 5. RF Processing

Estimation of the average velocity (Doppler frequency) after demodulation in a system with a high spatial resolution requires correction for the effects of depth and frequency dependent attenuation and will also make the velocity estimate more noise sensitive, because of the decreased SNR. Because of these problems a switch is made to direct processing of the received radio frequency (rf) signals, captured digitally with a relatively high conversion frequency. The average displacement of reflectors within a depth window over repeated observations then follows from the location of the peak of the cross-correlation [35] of the two-dimensional rf matrix $r(l, d)$:

$$\hat{C}(\delta) = \sum_{l} \sum_{d} r(l, d) r(l + 1, d + \delta). \tag{5.1}$$

As opposed to conventional Doppler processing, averaging is performed over the cross-correlation of subsequent rf signals over a depth window rather than correlation between rf signal and reference (oscillator) signal. The quality of the estimate improves with the length of the windows, in both depth (axial length sample volume) and time (PRF). The problem is to find the location of the peak. The rate of oversampling of the rf signal is reflected in the number of sample points within the main lobe of the cross-correlation function: a high oversampling is required to get a detailed cross-correlation [36]. This will put a high demand on processing power, also because for each sample point in depth the reflections of stationary and slowly moving reflectors should be removed prior to cross-correlation. A simple way to perform the latter operation is the removal of the baseline off-set, as observed over the time-window, but also higher order approaches have been suggested [37–

39]. To estimate precisely the displacement from a coarsely sampled cross-correlation function, various interpolation algorithms have been considered [40], but they all incorporate to some extent the anticipated shape of the auto-correlation of a received echo which may vary with the fractional bandwidth of the rf signal. The result of the above rf processing is a direct estimate of the average displacement, expressed in terms of the sampling distance in depth direction. In this approach the reference is the previously observed rf signal rather than an oscillator signal, eliminating the need for center frequency estimation and scaling. Most importantly the displacement estimate tends to work properly, even under poor SNR conditions (0 dB with the signal and noise levels based on the same spectral range). The phase detector in traditional pulse Doppler systems smoothes phase transitions prior to velocity estimation, while the rf processing technique retains in the displacement detection algorithm the information on phase transitions originating from the randomly distributed scatterers [24] by reversing the sequence of operations and selective averaging in the depth direction (Eq. (5.1)).

The cross-correlation function of a periodic (rf) signal exhibits the same periodicity, causing side lobes. For narrow band signals (ultrasound bursts containing several periods) these side lobes may incidentally attain higher values than the main lobe, resulting in displacement aliasing. However, employing short pulses will cause rapid decorrelation and attenuates the side lobes. That is why this approach is especially suited for displacement (velocity) estimation in systems with a high spatial resolution.

A weak point of the displacement estimation as outlined above is the required range of correlation lags, spanning a displacement range of one to two wavelengths. However, the number of required lags can be reduced to 3 if the rf signals are converted to a complex signal and the shape of the rf spectrum is known [41]. Because of the frequency characteristics of ultrasound transducers the spectral power density distribution $G(f)$ can be approximated by a Gaussian shape modeled as:

$$G(f) = \frac{2(N+S)}{B\sqrt{2\pi}} \exp\left(\frac{-2(f-f_c)^2}{B^2}\right). \tag{5.2}$$

It is thereby assumed that due to dedicated filtering the signal power $S$ and noise power $N$ cover the same root-mean square (RMS) frequency range $B$ around a center frequency $f_c$. The two-dimensional cross-correlation function $C(\tau, \delta)$, as function of the time lag $\tau$ and depth lag $\delta$ (both in seconds), will be the inverse Fourier transform of the power spectral distribution

(Wiener-Khinchin relation), taking into account the time shift $\delta'$ due to the displacement $\Delta x = v\tau = c\delta'/2$ of the scatterers with velocity $v$ towards the transducer in between observations:

$$C(\tau, \delta) = \int_0^\infty G(f) \exp\{2\pi f j(\delta + 2v\tau/c)\} df. \tag{5.3}$$

The basic transformation for a Gaussian pulse is:

$$F^{-1}\left[\exp(-af^2)\right] = \exp(-at^2). \tag{5.4}$$

Then the autocorrelation function ($\tau = 0$) is given by:

$$C(0, \delta) = \frac{2(N+S)}{B\sqrt{2\pi}} \exp\left(\frac{-2\delta^2}{B^2}\right) \exp\{2\pi j f_c \delta\} \tag{5.5}$$

and the cross-correlation function for $\tau \neq 0$ by:

$$C(\tau, \delta) = \frac{2S}{B\sqrt{2\pi}} \exp\left(\frac{-2(\delta + 2v\tau/c)^2}{B^2}\right) \exp\{2\pi j f_c(\delta + 2v\tau/c\}). \tag{5.6}$$

At this point the conversion can be made to discrete correlation coefficients by considering sampling in depth and in time. The rf signal is sampled with a frequency $f_s$ which should be a factor 4 higher than the central frequency $f_c$ to accommodate high frequency signals, because of the bandwidth $B$, [41]. This sets the unit of the depth lag to $\delta = 1/f_s$. The temporal sampling interval equals 1/PRF. Eq. (5.6) contains 5 unknown variables ($v$, $f_c$, $B$, $S$, $N$) which can be solved by considering the estimates for $C(0,0)$, $C(1,0)$ and $C(0,1)$

$$C(0,0) = \frac{2(S+N)}{B\sqrt{2\pi}}, \tag{5.7}$$

$$C(0,1) = \frac{2(S+N)}{B\sqrt{2\pi}} \exp\left(\frac{-2}{f_s^2 B^2}\right) \exp\{2\pi j f_c/f_s), \tag{5.8}$$

$$C(1,0) = \frac{2S}{B\sqrt{2\pi}} \exp\left(\frac{-8v^2}{B^2 c^2 \mathrm{PRF}^2}\right) \exp\{4\pi j f_c v/c\mathrm{PRF})\}. \tag{5.9}$$

The argument of the estimate for the autocorrelation coefficient provides the estimate for the center frequency of the received signal, while the argument of the estimate for the cross-correlation coefficient, normalized for the

estimated center frequency, gives the velocity:

$$\begin{aligned} \hat{f}_c &= f_s \arg\{\hat{C}(0,1)\}/2\pi\,, \\ \hat{v} &= \frac{c\mathrm{PRF}}{2f_s}\frac{\arg\{\hat{C}(1,0)\}}{\arg\{\hat{C}(0,1)\}}\,, \end{aligned} \tag{5.10}$$

$$\begin{aligned} \hat{B} &= \frac{\sqrt{2}}{f_s\sqrt{\ln\hat{C}(0,0) - \ln\left|\hat{C}(0,1)\right|}}\,, \\ \frac{S}{N} &= \frac{\left|\hat{C}(1,0)\right|}{\hat{C}(0,0)\exp\left(\frac{-8v^2}{B^2c^2\mathrm{PRF}^2}\right) - \left|\hat{C}(1,0)\right|}\,. \end{aligned} \tag{5.11}$$

The estimates for the center frequency, the bandwidth and the SNR can be used to validate the velocity estimate, e.g. if the SNR exceeds a given threshold the estimate is accepted, otherwise it will be zero. The cross-correlation coefficients of the complex rf signals, obtained via a Hilbert filter, within a data matrix with dimensions NS in depth and PL in time are estimated as:

$$\hat{C}(\tau,\delta) = \frac{\sum_{d=1}^{\mathrm{NS}-\delta}\sum_{t=1}^{\mathrm{NP}-\tau} r(t,d)r^x(t+\tau,d+\delta)}{(\mathrm{NS}-\delta-1)(\mathrm{PL}-\tau-1)}\,. \tag{5.12}$$

To get the best performance, the length of the depth window is set to the axial resolution of the system as follows from the estimates for center frequency and bandwidth. Simulations have shown (Fig. 9b) that the above estimator based on complex correlation function has a precision of less than 1% of the PRF for an rf signal with a fractional bandwidth of 0.5 for a wide range of signal conditions [41]. To improve robustness and detail in the velocity distribution, data windows are chosen half-overlapping in depth and in time, rendering a large number of velocity estimates per second for a depth range of 1–2 cm.

The common wall filter is a highpass filter and, hence, suppresses Doppler frequencies within a range around zero frequency. Considering a slowly moving structure like a vessel wall (or its reverberations within the lumen), the cut-off frequency and roll-off should be set high to avoid that in the early systolic phase the filter will leak signals from the structure. Clearly a zero order filter (removing the mean level) will not do. An alternative is to use above velocity estimator (Eq. (5.10)) estimator prior to wall filtering [42].

Then the signals of structures will dominate and the estimator provides the Doppler shift frequency as function of time, providing simultaneously information about the displacement of wall structures over time [42]. The wall Doppler shift is subsequently used to shift the complex rf signals in frequency, maintaining the spectral peak of the Doppler signals at zero frequency and allowing the highpass filter to function optimally. Since the spectral dispersion of the structures is limited, the selection of the cut-off frequency is only limited by the length of the time-window [27, 28, 43, 44]. After blood velocity detection the estimated velocities have to be corrected for the imposed shift in signal frequency.

Processing of rf data puts some demands on the echo-systems. First of all the rf signal should be accessible, while the phase relationship between emission and data capture is maintained. Moreover, the echo system should be capable to operate in echo M-mode with a high PRF (10 kHz for a 7.5 MHz system) to avoid frequency aliasing. Finally, capturing rf signals at a sample rate of 4 times the expected carrier frequency (25 MHz) at a PRF of 10 kHz over a range of 20 mm, covering an artery) produces a huge amount of data over an observation time of a few seconds.

## 6. Shear Stress

The shear stress is the drag per unit area exerted by the endothelium on the flowing blood. This will slow down the velocity of the blood close to the wall and for a straight vessel without bifurcations eventually result in a velocity distribution across the lumen with the highest velocity in the center of the lumen. A steep velocity gradient at the wall-lumen interface, indicated as shear rate (SR), corresponds to a high shear stress (SS):

$$\mathrm{SS} = \eta \left.\frac{\partial v(r)}{\partial r}\right|_{r=R} = \eta \mathrm{SR} \quad [\mathrm{Pa}]. \tag{6.1}$$

The blood viscosity $\eta$ varies with the shear rate: a low mean wall shear rate ($r = R$) causes a high blood viscosity. Especially at low shear rates (below $200\,\mathrm{s}^{-1}$) the viscosity will increase sharply, rendering viscosity measurements by means of a blood sample impractical. However, for physiological shear rates the non-Newtonian character of blood can be accounted for using plasma viscosity ($\eta_0$ [Pa s]), haemotocrit (Ht [%]) and wall shear rate, [45]:

$$\log(\eta) = \log(\eta_0) + (0.03 - 0.0076 \log(\mathrm{SR}))\mathrm{Ht}. \tag{6.2}$$

If we assume that the emitted ultrasound burst has effectively a length of 2 periods (a relative bandwidth of 0.5) and the received rf signal has a center frequency of 6.1 MHz, the length of the sample volume will be on the order of 0.25 mm which matches the anticipated beamwidth of 1 mm within the focal zone of a transducer. Processing the rf data in half-overlapping segments in depth and in time results in an interspacing of 0.125 mm, thereby retaining the spatial and temporal details in the velocity distribution (Fig. 11). As stated in the previous section, a wall filter adapting dynamically to the velocities of the artery walls allows detection of low velocities which may occur close to the vessel wall. These velocities may behave erratically, because velocity estimates have been set to zero based on the observed SNR while other velocity estimates have been accepted although they have an unreliable value. Smoothing with a $3 \times 3$ median filter preserves the edges of the velocity distribution. The next step is to compute the radial derivative of the observed velocity distribution for each time instant and at each site, starting from the middle of the lumen, resulting in the time-dependent shear rate distribution. Near the wall the shear rate will attain the highest value and the maximum within a range of 2 mm is accepted as the wall shear rate, [42]. As a consequence the position at which the wall shear rate is obtained dynamically varies over the cardiac cycle with the motion of the walls (Fig. 11). To reduce minor curvature effects and associated secondary flow effects, the wall shear rates at the near and far wall (from the viewpoint of the ultrasound transducer) are averaged.

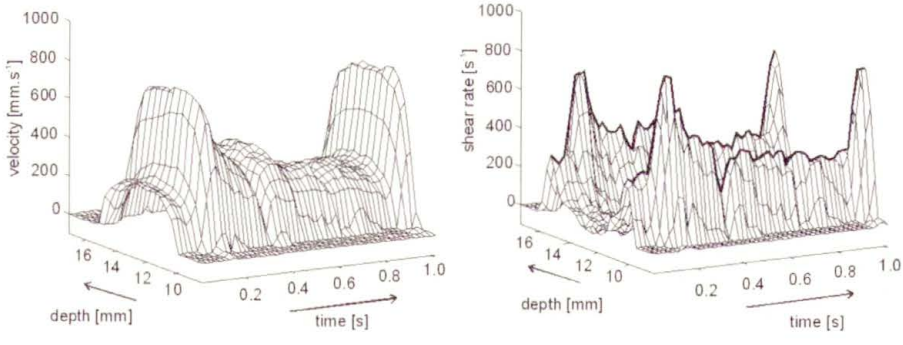


(a) (b)

FIGURE 11. Time-dependent velocity (left) and shear rate (right) distribution in the common carotid artery of a young volunteer

Although the adaptive wall filter permits the detection of relatively low velocities, it remains impossible to detect the velocity gradient exactly at the wall lumen interface, also because computation of the velocity gradient involves 2 neighboring sample volumes with a non-zero velocity estimate. For a 7.5 MHz system the actual velocity gradient is computed at a distance of 0.3 mm from the wall [46]. For an artery with a diameter of 6 mm, this will cause an underestimation of the true velocity gradient on the order of 10%. On the other hand it may be assumed that at that radial position the effects of shear thinning are negligible and that the estimated whole blood viscosity (Eq. (6.2)) can be used.

One may consider using color Doppler systems in color M-mode (Sec. 7) to assess the time-dependent wall shear rate. These systems, however, have a poor spatial resolution, because they employ long ultrasound bursts (Sec. 1) in Doppler mode. Moreover, the wall filters are not balanced to effectively separate Doppler signals from the wall and from the blood with about the same velocity relative to the ultrasound transducer. Generally the wall filter is the key problem to assess the velocity gradient close to the wall. Let us assume that the cut-off frequency of the filter corresponds to a velocity of 3 cm/s, then the minimal velocity gradient for consecutive sample volumes spaced at 0.3 mm equals $100\,\mathrm{s}^{-1}$. Only if the velocity gradient is higher than this estimated value it can be attributed to the velocity distribution.

Since it remains problematic to measure directly the time-dependent wall shear rate researchers evaded to indirect methods, [47–50]. For a steady flow the velocity distribution in a straight vessel will eventually develop a parabolic shape, provided that the entrance length is sufficiently long. Then the wall shear rate is directly related to the center stream velocity $v$ which can easily be measured with available Doppler systems [51]:

$$\mathrm{SR} = 2nv/D. \tag{6.3}$$

In this expression $D$ stands for the lumen diameter and $n$ indicates the exponent of the modeled velocity distribution (which is 2 for a parabolic velocity profile). For dynamic pulsatile conditions the shape of the velocity distribution will vary over the cardiac cycle, but it is assumed that the mean shape is still parabolic. However, direct comparison between direct and indirect measurements shows that the indirect method underestimates the mean and peak-systolic shear rate, and, hence, peak and mean wall shear stress, especially for compliant vessels, [52]. For elastic arteries the exponent is higher than 3, indicating a blunted velocity profile.

It is generally accepted that the lumen diameter is adjusted to the prevailing shear stress, [53–56]. At high shear stresses the endothelium will produce vasodilating agents, like NO and prostacyclines [57], increasing arterial diameter and, hence, keeping the shear stress within limits. At a low shear stress, however, less of these vasodilating autocoids and endotheline (a vasoconstricting agent) will be released, causing vasoconstriction. It is assumed that regulation of the shear stress eventually results in a mean shear stress of 1.5 Pa (15 dyne/cm$^2$). In the common carotid artery we indeed observed shear stresses of about 1.3 Pa, but in the brachial [52] and the femoral [58] artery substantially lower mean stresses were found, ranging between 0.5 and 0.3 Pa. The latter arteries supply vascular beds with a high variation in blood demand (factor 20–30), depending on the level of exercise, and an associated variation in peripheral resistance. For this condition it is virtually impossible to adjust dynamically the artery diameter to retain a shear stress of 1.5 Pa. A high shear stress may after all damage the endothelium, [59]. That is why arteries in the extremities have a substantially lower mean shear stress at rest, [50, 60] to accommodate without endothelial damage the high blood flow in exercise.

## 7. Color Doppler Imaging

Blood cells exhibit a low echogenicity compared to structures like vessel walls. Consequently blood appears black on an echo-image, but by using the brightness information it is rather easy to locate normal arteries using. The situation changes for arteries with calcified walls and a suspected low or absent blood flow. Moreover, thrombotic formations as a result of vulnerable plaques have a higher echo level than blood and the difference with vessel walls is not so obvious anymore. That is why some decades ago it was proposed to extend the potentials of multigate Doppler systems to 2-dimensional flow maps where the velocity information is superimposed in color (color Doppler) on the echo-image in B-mode, [23]. The direct visualization of the anatomical relationship between structures and flow makes it directly clear where anomalies are to be expected.

To obtain flow maps a large number of sample volumes distributed along the ultrasound beam have to be repetitively interrogated in pulsed Doppler mode. An observation time of 1 ms (4 to 8 subsequent emission and processing cycles) will do to obtain a crude estimate for the velocity distribution

[15, 26, 28, 61–69], whereafter the beam is switched to another direction and the process is repeated. In this way 16 velocity maps composed of 64 lines can be produced per second. Although pulsed Doppler processing is subject to aliasing, it does not seem to be a problem for color mode systems because aliasing artifacts will show up as a mosaic pattern: the random distribution of high velocities with opposite directions are easily identified as jets with a high velocity as may occur in and distal to stenotic heart valves and artery stenoses.

Large flow maps composed of many lines or a low PRF because of the required depth of investigation will reduce the flow map rate to below 10 frames per second, which becomes prohibitive to fully appreciate the dynamic behavior of arterial flow and cardiac action. That is why for the flow map, preference is given to a subsector of the echo-image, which is also intermittently updated. Because of the short observation time, the estimated velocities are rather noisy prohibiting numeric quantification. Moreover the short observation time sets a lower limit to the cut-off frequency of the vessel wall filter, leaving a void between the color map and the wall. For a more accurate assessment of flow anomalies the system is switched to single M-line color mode or to single gate Doppler permitting frequency analysis of a sample volume positioned, using the echo and flow map information.

It may depend on the application, but in most situations one is interested in the presence of blood flow rather than its magnitude. For those situations it is not necessary to calculate the velocity map: it is sufficient to detect the amplitude of the Doppler signals [70–74] and to display its 2-dimensional distribution in color mode (power Doppler, angio Doppler). A drawback is that the information about flow direction is lost. On the other hand one may average over a longer time, reducing estimation artifacts in the image.

## 8. Conclusions

Color Doppler systems differentiate the flow direction with a color (red or blue) while the flow velocity is indicated by the brightness of the color. The question remains whether the color is indeed linked to the sign of the observed Doppler shift or to the type of vessel (artery or vein). In Sec. 1 it was argued that particles moving towards the transducer would induce a positive Doppler shift, but at many stages within a Doppler system the assigned phase relationship is rather arbitrary. This applies to the reference signals for

the demodulator (Sec. 2.1), for the inputs of the velocity estimator (Sec. 2.3) and for the audio signal separator (Sec. 2.2). If the inputs are swapped the system still functions properly, although the sign of the velocity output will be reversed. The situation becomes even more complicated for rf processing (Sec. 5). There the direction of the displacement is linked to the time elapsed after emission: a positive displacement is then associated with a shift to a greater depth. For Eq. (5.3) this was corrected for by assigning to the time-shift, due to a negative displacement (motion towards the transducer), with a positive sign, while strictly speaking the sign should be negative.

Also in their application Doppler systems are not consistent. Spectra are most easily interpreted if they are displayed in a positive fashion. Whether arteries are interrogated with the probe direction aligned with the suspected flow direction or rather in the opposite direction depends on the local anatomy. It is easier to observe the carotid arteries with the probe directed towards the head, while in the brachial arteries the probe direction is opposed to the main flow direction. But arteries may also exhibit a reversed flow direction. A well-known example is the flow direction in the ophthalmic artery, which changes sign if the blood pressure in the cerebral circulation is relatively low due to an obstruction in the internal carotid artery. Also the flow direction in the right common carotid artery may be reversed if the brachiocephalicus (connecting the aorta to the right carotid artery and the subclavian artery) is occluded. Then the right arm is indirectly supplied by flow from the head.

Because of the reported ambiguities in hardware, application and disease it is nice that Doppler systems are equipped with a switch to change the polarity of the observed velocities. Color Doppler systems do not color arteries red, however, it is the user who determines the displayed polarity, i.e. the assignment of the red and blue color.

## References

1. T. YOSHIDA, M. MORI, Y. NIMURA, G. HIKITA, S. TAKA GISHI, K. NAKANISHI and S. SATOMURA, *Analysis of heart motion with ultrasonic Doppler method and its clinical application*, Am Heart J, **61**: 61–75, 1961.

2. D.L. FRANKLIN, W. SCHLEGEL and R.F. RUSHMER, *Blood flow measured by Doppler frequency shift of back-scattered ultrasound*, Science, **134**: 564–565, 1961.

3. C. DOPPLER, *Ueber das farbige Licht der Dopplesterne und einige anderer Gestirne des Himmels*, presented at Gesellschaft der Wissenschaften, Prag, 25 Mai, 1842.

4. C.H.D. BUIJS BALLOT, *Akustische Versuche auf der Niederländische Eisenbahn, nebst gelegentlichen bemerkingen zur Theorie des Hrn Prof. Doppler*, Annalen Physik Chemie, **66**: 321–351, 1845.

5. R.S. RENEMAN and M.P. SPENCER, *Local Doppler audio spectra in normal and stenosed carotid arteries in man*, Ultrasound Med Biol, **5**(1): 1–11, 1979.

6. D. GABOR, *Theory of communications*, Journal IEE, **93**: 429–457, 1946.

7. R.S. RENEMAN, H.F. CLARKE, N. SIMMONS, and M.P. SPENCER, *In vivo comparison of electromagnetic and Doppler flowmeters: with special attention to the processing of the analogue Doppler flow signal*, Cardiovasc Res, **7**: 557–566, 1973.

8. P.J. FISH, P.R. HOSKINS, C. MORAN and W.N. MCDICKEN, *Developments in cardiovascular ultrasound. Part I: signal processing and instrumentation*, Med Biol Erg Comput, **35**: 561–569, 1997.

9. P.A. PERONNEAU, J.P. BOURNAT, A. BUGNON, A. BARBET and M. XHAARD, *Theoretical and practical aspects of pulsed Doppler flowmetry: real-time applications to the measure of instantaneous velocity profiles*, [in:] Cardiovascular applications of ultrasound, R.S. Reneman, [Ed.], pp.66–84, Amsterdam-London: North-Holland Publ. Co., 1974.

10. R.W. GILL, *Performance of the mean frequency Doppler modulator*, Ultrasound Med Biol, **5**: 237–247, 1979.

11. A.P.G. HOEKS, M. HENNERICI and R.S. RENEMAN, *Spectral composition of Doppler signals*, Ultrasound Med Biol, **17**: 751–760, 1991.

12. D.G. PAENG, R.Y. CHIAO and K.K. SHUNG, *Echogenicity variations from porcine blood I: the "bright collapsing ring" under pulsatile flow*, Ultrasound Med Biol, **30**: 45–55 2004.

13. D.G. PAENG and K.K. SHUNG, *Cyclic and radial variation of the Doppler power from porcine whole blood*, IEEE Trans Ultrason Ferroelectr Freq Control, **50**: 614–622, 2003.

14. D. PAENG, P. CAO and K.K. SHUNG, *Doppler power variation from porcine blood under steady and pulsatile flow*, Ultrasound Med Biol, **27**: 1245–1254, 2001.

15. P.R. HOSKINS, *A review of the measurement of blood velocity and related quantities using Doppler ultrasound*, Proc Inst Mech Eng, **213**: 391–400, 1999.

16. P.R. HOSKINS, P.J. FISH, W.N. MCDICKEN and C. MORAN, *Developments in cardiovascular ultrasound. Part 2: arterial applications*, Med Biol Eng Comput, **36**: 259–269, 1998.

17. R. MORAES, N. AYDIN and D.H. EVANS, *The performance of three maximum frequency envelope detection algorithms for Doppler signals*, J. Vasc. Invest., **1**: 126–134, 1995.

18. K. MARASEK and A. NOWICKI, *Comparison of the performance of three maximum Doppler frequency estimators coupled with different spectral estimation methods*, Ultrasound Med Biol, **20**: 629–638, 1994.

19. L.Y.L. MO, L.C.M. YUN and R.S.C. COBBOLD, *Comparison of four digital maximum frequency estimators*, Ultrasound Med Biol, **14**:355–363, 1988.

20. A. NOWICKI, P. KARLOWICZ, M. PIECHOCKI and W. SECOMSKI, *Method for the measurement of the maximum Doppler frequency*, Ultrasound Med Biol, **11**:479–486, 1985.

21. T. D'ALESSIO, *Objective algorithm for maximum frequency estimation in Doppler spectral analysers*, Med Biol Eng Comput, **23**:63–68, 1985.

22. A.P.G. HOEKS, C.J. RUISSEN, P. HICK and R.S. RENEMAN, *Methods to evaluate the sample volume of pulsed Doppler systems*, Ultrasound Med Biol, **10**:427–434, 1984.

23. C. KASAI, K. NAMEKAWA, A. KOYANO and R. OMOTO, *Real-time two-dimensional blood flow imaging using an autocorrelation technique*, IEEE Trans Son Ultrason, **SU-32**:458–464, 1985.

24. A.P.G. HOEKS, T.G.J. ARTS, P.J. BRANDS and R. S. RENEMAN, *Comparison of the performance of the cross correlation and Doppler autocorrelation technique to estimate the mean velocity of simulated ultrasound signals*, Ultrasound Med Biol, **19**:727–740, 1993.

25. T. LOUPAS, J.T. POWERS and R.W. GILL, *An axial velocity estimator for ultrasound blood flow imaging, based on a full evaluation of the Doppler equation by means of a two-dimensional autocorrelation approach*, IEEE Trans Ultrason Ferroelectrics Freq Control, **42**:672–688, 1995.

26. H. TORP, K. KRISTOFFERSEN and B.A.J. ANGELSEN, *Autocorrelation techniques in color flow imaging: signal model and statistical properties of the autocorrelation estimates*, IEEE Trans Ultrason Ferroelectrics Freq Control, **41**:604–612, 1994.

27. L.A.F. LEDOUX, P.J. BRANDS and A.P.G. HOEKS, *Reduction of the clutter component in Doppler ultrasound signals based on singular value decomposition: a simulation study*, Ultrason Imaging, **19**:1–18, 1997.

28. H. TORP, *Clutter rejection filters in color flow imaging: a theoretical approach*, IEEE Trans Ultrason Ferroelectrics Freq Control, **44**:417–424, 1997.

29. M. BRANDESTINI, *Topoflow—a digital full range Doppler velocity meter*, IEEE Trans. Sonics and Ultrasonics, **SU-25**:287–293, 1978.

30. A.P.G. HOEKS, R.S. RENEMAN and P.A. PERONNEAU, *A multi-gate pulsed Doppler system with serial data processing*, IEEE Trans. Sonics Ultrason, **SU-28**:242–247, 1981.

31. P. TORTOLI, F. GUIDI, G. GUIDI and C. ATZENI, *Spectral velocity profiles for detailed ultrasound flow analysis*, IEEE Trans Ultrason Ferroelectrics Freq Control, **43**:654–658, 1996.

32. R.S. RENEMAN, T. VAN MERODE, P. HICK and A.P.G. HOEKS, *Flow velocity patterns in and distensibility of the carotid artery bulb in subjects of various ages*, Circulation, **71**:500–509, 1985.

33. R.S. RENEMAN, T. VAN MERODE, P. HICK and A.P.G. HOEKS, *Cardiovascular applications of multi-gate pulsed Doppler systems*, Ultrasound Med Biol, **12**: 357–370, 1986.

34. S.I. RABBEN, S. BAERUM, V. SORHUS and H. TORP, *Ultrasound-based vessel wall tracking: an auto-correlation technique with RF center frequency estimation*, Ultrasound Med Biol, **28**: 507–517, 2002.

35. O. BONNEFOUS and P. PESQUE, *Time domain formulation of pulse-Doppler ultrasound and blood velocity estimation by cross correlation*, Ultrason Imaging, **8**: 73–85, 1986.

36. J.A. JENSEN, *Range/velocity limitations for time-domain velocity estimation*, Ultrasound Med Biol, **19**: 741–749, 1993.

37. A.P.G. HOEKS, J.J.W. VAN DE VORST, A. DABEKAUSSEN, P. J. BRANDS and R.S. RENEMAN, *An efficient algorithm to remove low frequency Doppler signals in digital Doppler systems*, Ultrason Imaging, **13**: 135–144, 1991.

38. J.A. JENSEN, *Stationary echo canceling in velocity estimation by time-domain cross-correlation*, IEEE Trans Ultrason Ferroelectrics Freq Control, **12**: 471–477, 1993.

39. M. SCHLAIKJER, S. TORP-PEDERSEN and J.A. JENSEN, *Simulation of RF data with tissue motion for optimizing stationary echo canceling filters*, Ultrasonics, **41**: 415–419, 2003.

40. X. LAI and H. TORP, *Interpolation methods for time-delay estimation using cross-correlation method for blood velocity measurement*, IEEE Trans Ultrason Ferroelectrics Freq Control, **46**: 277–290, 1999.

41. P.J. BRANDS, A.P.G. HOEKS, L.A.F. LEDOUX and R. S. RENEMAN, *A radio frequency domain complex cross-correlation model to estimate blood flow velocity and tissue motion by means of ultrasound*, Ultrasound Med Biol, **23**: 911–920, 1997.

42. P.J. BRANDS, A.P.G. HOEKS, J. WILLIGERS, C. WILLEKES and R.S. RENEMAN, *An integrated system for the non-invasive assessment of vessel wall and hemodynamic properties of large arteries by means of ultrasound*, Eur. J. Ultrasound, **9**: 257–266, 1999.

43. S. BJAERUM, H. TORP and K. KRISTOFFERSEN, *Clutter filters adapted to tissue motion in ultrasound color flow imaging*, IEEE Trans Ultrason Ferroelectrics Freq Control, **49**: 693–704, 2002.

44. Y.M. YOO, R. MANAGULI and Y. KIM, *Adaptive clutter filtering for ultrasound color flow imaging*, Ultrasound Med Biol, **29**: 1311–1320, 2003.

45. J.P.A. WEAVER, A. EVANS and D.N. WALDER, *The effect of increased fibrinogen content on the viscosity of blood*, Clin Sci, **36**: 1–10, 1969.

46. F.J.H. GIJSEN, P.J. BRANDS, F.N. VAN DE VOSSE and J. D. JANSSEN, *Assessment of wall shear rate measurements with ultrasound*, J. Vasc. Invest., **4**: 187–196, 1998.

47. A. GNASSO, C. IRACE, C. CARALLO, M.S. DE FRANCESCHI, C. MOTTI, P.L. MATTIOLI and A. PUJIA, *In vivo association between low wall shear stress and plaque in subjects with asymmetrical carotid atherosclerosis*, Stroke, **28**: 993–998, 1997.

48. A. GNASSO, C. CARALLO, C. IRACE, V. SPAGNUOLO, G. DE NOVARA, P.L. MATTIOLO and A. PUJIA, *Association between intima-media thickness and wall shear stress in common carotid artery in healthy male subjects*, Circulation, **94**: 3257–3262, 1996.

49. A. GNASSO, C. CARALLO, C. IRACE, M.S. DE FRANCESCHI, P. L. MATTIOLI, C. MOTTI and C. CORTESE, *Association between wall shear stress and flow-mediated vasodilation in healthy men*, Atherosclerosis, **156**: 171–176, 2001.

50. A. SCHMIDT-TRUCKSASS, A. SCHMID, C. BRUNNER, N. SCHERER, G. ZACH, J. KEUL and M. HUONKER, *Arterial properties of the carotid and femoral artery in endurance- trained and paraplegic subjects*, J Appl Physiol, **89**: 1956–1963, 2000.

51. A.P.G. HOEKS and R.S. RENEMAN, *Flow patterns and arterial wall dynamics*, [in:] Cerebrovascular ultrasound, M.G. Hennerici and S.P. Meairs, [eds.], pp.77–87, Cambridge: University Press, 2001.

52. R. DAMMERS, F. STIFFT, J.H. TORDOIR, J.M. HAMELEERS, A.P. HOEKS and P.J. KITSLAAR, *Shear stress depends on vascular territory: comparison between common carotid and brachial artery*, J. Appl. Physiol., **94**: 485–489, 2003.

53. C.D. MURRAY, *The physiological principle of minimum work. I: The vascular system and the cost of blood volume*, Proc. Nat. Acad. Sci. USA, **12**: 207–214, 1926.

54. A. KAMIYA, R. BUKHARI and T. TOGAWA, *Adaptive regulation of wall shear stress optimizing vascular tree function*, Bulletin Math Biol, **46**: 127–137, 1984.

55. M. ZAMIR, P. SINCLAIR and T.M. WONNACOTT, *Relation between diameter and flow in major branches of the aorta*, J. Biomech., **25**: 1303–1310, 1992.

56. C.K. ZARINS, M.A. ZATINA, D.P. GIDDENS, D.N. KU and S. GLAGOV, *Shear stress regulation of artery lumen diameter in experimental atherogenesis*, J. Vasc. Surg., **5**: 413–420, 1987.

57. R. BUSSE and I. FLEMING, *Pulsatile stretch and shear stress; physical stimuli determining the production of endothelium-derived relaxing factors*, J. Vasc. Res., **35**: 73–84, 1998.

58. L. KORNET, A.P. HOEKS, J. LAMBREGTS and R.S. RENEMAN, *Mean wall shear stress in the femoral arterial bifurcation is low and independent of age at rest*, J. Vasc. Res., **37**: 112–122, 2000.

59. M.R. ROACH and N.B. SMITH, *Does high shear stress induced by blood flow lead to atherosclerosis*, Persp Biol Medicine, **26**: 287–303, 1983.

60. P.C. DE GROOT, F. POELKENS, M. KOOIJMAN and M.T. HOPMAN, *Preserved flow-mediated dilation in the inactive legs of spinal cord-injured individuals*, Am. J. Physiol. Heart Circ. Physiol., **287**: H374–380, 2004.

61. D.F. SWITZER and N.C. NANDA, *Doppler color flow mapping*, Ultrasound Med Biol, **11**: 403–416, 1985.

62. A. KURJAK, Z. ALFIREVIC and M. MILJAN, *Conventional and color Doppler in the assessment of fetal and maternal circulation*, Ultrasound Med. Biol., **14**:337–354, 1988.

63. J. HOLEN, M. NANA, J. LOCKHART and R. WAAG, *Doppler color flow in echocardiography: analytical and in-vitro investigations of the quantitative relationship between orifice flow and color jet dimension*, Ultrasound Med. Biol., **16**:543–551, 1990.

64. A. KITABATAKE, J. TANOUCHI, Y. YOSHIDA, T. MASUYAMA, M. UEMATSU and T. KAMADA, *Quantitative color flow imaging to measure the two-dimensional distribution of blood flow velocity and the flow rate*, Jap. Circulation J., **54**:304–308, 1990.

65. W. STEINKE, H. KLOETZSCH and M. HENNERICI, *Carotid artery disease assessed by color Doppler flow imaging. Correlation with standard Doppler sonography and angiography*, AJNR, **11**:259–266, 1990.

66. C. RANKE, U. HENDRICKX ROTH, F. BRASSEL, A. CREUTZIG and K. ALEXANDER, *Color and conventional image-directed Doppler ultrasonography: accuracy and sources of error in quantitative blood flow measurements*, J. Clin. Ultrasound, **20**:187–193, 1992.

67. P.N.T. WELLS, *Today's state of the art: does colour velocity imaging overtake colour Doppler?*, J. Vasc. Investigation, **1**:38–43, 1995.

68. A. HERMENT, G. DEMOMENT and P. DUMÉE, *Improved estimation of low velocities in color Doppler imaging by adapting the mean frequency estimator to the clutter rejection filter*, IEEE Trans Biomed Eng, **43**:919–927, 1996.

69. K. FERRARA and G. DEANGELIS, *Color flow mapping*, Ultrasound Med Biol, **23**:321–345, 1997.

70. M.A. MOEHRING and M.P. SPENCER, *Power M-mode Doppler (PMD) for observing cerebral blood flow and tracking emboli*, Ultrasound Med Biol, **28**:49–57, 2002.

71. M. BRUCE, M. AVERKIOU, K. TIEMANN, S. LOHMAIER, J. POWERS and K. BEACH, *Vascular flow and perfusion imaging with ultrasound contrast agents*, Ultrasound Med Biol, **30**:735–743, 2004.

72. M. SAQQUR, N. DEAN, M. SCHEBEL, M.D. HILL, A. SALAM, A. SHUAIB and A.M. DEMCHUK, *Improved detection of microbubble signals using power M-mode Doppler*, Stroke, **35**:e14–17, 2004.

73. S. HUBER, R. STEINBACH, O. SOMMER, I. ZUNA, H. CZEMBIREK and S. DELORME, *Contrast-enhanced power Doppler harmonic imaging-influence on visualization of renal vasculature*, Ultrasound Med. Biol., **26**:1109–1115, 2000.

74. L. ALLARD and G. CLOUTIER, *Power Doppler ultrasound scan imaging of the level of red blood cell aggregation: an in vitro study*, J. Vasc. Surg, **30**:157–168, 1999.